curvature is odd in energy (*20*), $\sigma_{xy}$ has the same sign for both electrons and holes. This contrasts with the conventional Hall conductivity that is sign-changing under carrier-type reversal. As a result, $\sigma_{xy}$ given by Eq. 2 is less susceptible to smearing by inhomogeneity. This mechanism yields a nonzero $R_{NL}$ whenever the Fermi level is tuned through Berry curvature hot spots. Their extent in energy is given by half the bandgap $\Delta \approx 180$ K, which translates into $n \approx 2 \times 10^{10}$ cm$^{-2}$ and agrees well with the ultranarrow width of our $R_{NL}$ peaks.

Because of TRS, the electric field generates topological currents (Eq. 1) with opposite transverse components in graphene's two valleys, $K$ and $K'$ (Fig. 1A), to create the charge-neutral VHE, $J_v = J_K - J_{K'} = \sigma^v_{xy}E$, where $\sigma^v_{xy} = 2\sigma_{xy}$. As illustrated in the inset to Fig. 1B, topological currents can result in a VHE conductivity of $\approx 2e^2/h$. In the absence of intervalley scattering, the charge-neutral currents can persist over extended distances and mediate nonlocal electrical signals (*24*–*28*). The resulting nonlocal resistance $R_{NL}$ can be understood as originating from the VHE and a reverse VHE (*20*), by analogy with nonlocal transport mediated by charge-neutral spin or energy flow (*24*–*28*). Yet unlike the latter, the VHE-induced nonlocality appears without TRS breaking—that is, at zero $B$. This behavior, as well as the narrow range of $n$ over which $R_{NL}$ is observed, is a telltale sign of bulk topological currents. The analysis outlined above yields the model expression (*20*)

$$R_{NL} = (w/2\xi)(\sigma^v_{xy})^2\rho^3_{xx}\exp(-L/\xi) \qquad (3)$$

The peak in $R_{NL}(n)$ can be described by Eq. 3 with no fitting parameters (Fig. 2B).

The measured spatial decay with $\xi \approx 1.0$ μm is consistent with intervalley scattering occurring at graphene edges and/or at atomic-scale defects (*20*). The large values of $R_{NL}$ at $L$ of several micrometers also imply extremely strong topological currents locally, within the path of the applied current. By extrapolating the observed $L$ dependence to $L < 1$ μm, Fig. 2C yields $R_{NL}$ ~10 kilohm. According to Eq. 3, this translates into $\sigma^v_{xy} \approx 2e^2/h$ and order-one Hall angles, which is in agreement with the VHE expected for weak intervalley scattering. Furthermore, similar to classical magnetotransport, changes in the direction of current flow can lead to additional resistivity. For $\sigma_{xy}\rho_{xx} \sim 1$, the classical magnetoresistance reaches a value of $\sim\rho_{xx}$ when carriers of opposite sign are involved. A valley analog of this extra resistance may explain anomalous contributions of ~10 kilohm in $\rho_{xx}$, which are observed at short distances $L \approx w$ by using the bend geometry (fig. S7). Parenthetically, the intrinsic VHE mechanism discussed above, which provides excellent agreement with our experimental results, may coexist with extrinsic VHE mechanisms such as skew scattering and side jumps (*6*). Although their role in graphene superlattices remains to be examined, such mechanisms also originate from Berry curvature and arise under the same symmetry conditions as the intrinsic contribution.

Last, sharp changes in $R_{NL}$ with $V_g$ (130-nm-thick dielectric) (Figs. 1 and 2) amount to a transistor-like response with a slope of ≈100 mV/dec—that is, the detected voltage changes by a factor of 10 by varying $V_g$ by ≈100 mV. Although the peaks in $R_{NL}$ broaden with increasing $T$ and disappear above 100 K (because of the relatively small $\Delta$), one can envision electronic devices based on the valley degrees of freedom (*29*), which would become practical if larger bandgap values are achieved. To explore this further, we fabricated a superlattice device with a short top gate (15-nm dielectric) placed between the current and voltage contacts used for nonlocal measurements (fig. S8). Valley currents in this case could be switched on and off, similar to the case of a field effect transistor, by a gate voltage of ≈10 mV at 20 K (*20*). It is feasible to further reduce the thickness of the top gate hBN dielectric down to 2 nm, which would translate into a gate response down to <2 mV/dec at this $T$. Although further analysis is necessary, these results may indicate that subthreshold slopes better than those achievable for conventional charge-based processing devices (*30*) are possible.

## REFERENCES AND NOTES


1. W. Kohn, J. M. Luttinger, *Phys. Rev.* **108**, 590–611 (1957).
2. G. Sundaram, Q. Niu, *Phys. Rev. B* **59**, 14915–14925 (1999).
3. F. D. M. Haldane, *Phys. Rev. Lett.* **93**, 206602 (2004).
4. D. Xiao, W. Yao, Q. Niu, *Phys. Rev. Lett.* **99**, 236809 (2007).
5. D. Xiao, M.-C. Meng, Q. Niu, *Rev. Mod. Phys.* **82**, 1959–2007 (2010).
6. N. Nagaosa, J. Sinova, S. Onoda, A. H. MacDonald, N. P. Ong, *Rev. Mod. Phys.* **82**, 1539–1592 (2010).
7. J. Zak, *Phys. Rev. Lett.* **62**, 2747–2750 (1989).
8. C. L. Kane, E. J. Mele, *Phys. Rev. Lett.* **95**, 226801 (2005).
9. B. A. Bernevig, T. L. Hughes, S. C. Zhang, *Science* **314**, 1757–1761 (2006).
10. L. Fu, C. L. Kane, E. J. Mele, *Phys. Rev. Lett.* **98**, 106803 (2007).
11. R. Roy, *Phys. Rev. B* **79**, 195322 (2007).
12. M. König *et al.*, *Science* **318**, 766–770 (2007).
13. C. Z. Chang *et al.*, *Science* **340**, 167–170 (2013).
14. D. Hsieh *et al.*, *Science* **323**, 919–922 (2009).
15. D. Xiao, G. B. Liu, W. Feng, X. Xu, W. Yao, *Phys. Rev. Lett.* **108**, 196802 (2012).
16. K. F. Mak, K. L. McGill, J. Park, P. L. McEuen, *Science* **344**, 1489–1492 (2014).
17. T. Ando, T. Nakanishi, R. Saito, *J. Phys. Soc. Jpn.* **67**, 2857–2862 (1998).
18. B. Hunt *et al.*, *Science* **340**, 1427–1430 (2013).
19. C. R. Woods *et al.*, *Nat. Phys.* **10**, 451–456 (2014).
20. Materials and methods are available as supplementary materials on *Science* Online.
21. L. A. Ponomarenko *et al.*, *Nature* **497**, 594–597 (2013).
22. C. R. Dean *et al.*, *Nature* **497**, 598–602 (2013).
23. Z. G. Chen *et al.*, *Nat. Commun.* **5**, 4461 (2014).
24. D. A. Abanin *et al.*, *Science* **332**, 328–330 (2011).
25. J. C. W. Song, P. Samutpraphoot, L. S. Levitov, Topological bands in G/hBN heterostructures. http://arxiv.org/abs/1404.4019 (2014).
26. J. Renard, M. Studer, J. A. Folk, *Phys. Rev. Lett.* **112**, 116601 (2014).
27. M. Titov *et al.*, *Phys. Rev. Lett.* **111**, 166601 (2013).
28. D. A. Abanin, A. V. Shytov, L. S. Levitov, B. I. Halperin, *Phys. Rev. B* **79**, 035304 (2009).
29. A. Rycerz, J. Tworzydlo, C. W. J. Beenakker, *Nat. Phys.* **3**, 172–175 (2007).
30. S. M. Sze, K. K. Ng, *Physics of Semiconductor Devices* (Wiley, New York, 2007), chap. 6.


## ACKNOWLEDGMENTS

This work was supported by the European Research Council, the Royal Society, the Office of Naval Research, the Air Force Office of Scientific Research, the Engineering and Physical Sciences Research Council (UK), and the National Science Foundation.

## SUPPLEMENTARY MATERIALS

www.sciencemag.org/content/346/6208/448/suppl/DC1
Materials and Methods
Supplementary Text
Figs. S1 to S8
References (*31*–*37*)

17 April 2014; accepted 29 August 2014
Published online 11 September 2014;
10.1126/science.1254966

Downloaded from http://science.sciencemag.org/ on March 13, 2018

ASYMMETRIC CATALYSIS

# Room-temperature enantioselective C–H iodination via kinetic resolution

**Ling Chu, Kai-Jiong Xiao, Jin-Quan Yu***

**Asymmetric carbon-hydrogen (C–H) activation reactions often rely on desymmetrization of prochiral C–H bonds on the same achiral molecule, using a chiral catalyst. Here, we report a kinetic resolution via palladium-catalyzed enantioselective C–H iodination in which one of the enantiomers of a racemic benzylic amine substrates undergoes faster aryl C–H insertion with the chiral catalysts than the other. The resulting enantioenriched C–H functionalization products would not be accessible through desymmetrization of prochiral C–H bonds. The exceedingly high relative rate ratio ($k_{fast}/k_{slow}$ up to 244), coupled with the subsequent iodination of the remaining enantiomerically enriched starting material using a chiral ligand with the opposite configuration, enables conversion of both substrate enantiomers into enantiomerically pure iodinated products.**

A wide range of C–H activation reactions have emerged as promising tools for organic synthesis over the past two decades. However, the development of enantioselective C–H activation reactions has met with limited success in terms of efficiency and scope (*1*). Enantioselective carbene insertions into prochiral methylene C–H bonds adjacent to heteroatoms have been achieved in synthetically useful enantioselectivity (*2*). Asymmetric nitrene insertion has also been demonstrated in both diastereoselective and enantioselective

manners (*3*–*6*). Development of asymmetric C–H activation reactions involving a metal insertion step has also witnessed limited but encouraging progress. Combining C–H activation with subsequent asymmetric carbometalation onto double bonds elegantly connects C–H functionalization reactions to asymmetric catalysis (*7*, *8*). An early example of atropselective alkylation in moderate enantioselectivity [49% enantiomeric excess (ee)] was reported (*9*). Recently, Pd-catalyzed desymmetrization of prochiral C–H bonds has been achieved with excellent levels of enantioselectivity (*10*–*14*) (Fig. 1A). However, the requirement for the presence of two chemically identical groups necessarily limits the structural diversity of the chiral products, preventing the broad application of this method in asymmetric synthesis. An effort to overcome this limitation by developing enantioselective C–H activation of racemic mixtures via a regiodivergent pathway has been reported with an intramolecular reaction (*15*).

Chiral amines are one of the most prevalent motifs in bioactive natural products, drug compounds, and chiral catalysts. Despite remarkable progress in the development of catalytic enantioselective methods for synthesis of chiral amines (*16*), chiral auxiliaries (*17*), classical resolution by crystallization of chiral salts, and enzymatic kinetic resolution (*18*, *19*) are more often used in practice. Nonenzymatic kinetic resolution of amines by asymmetric acyl transfer catalysts remains a substantial challenge when compared to the analogous kinetic resolution of alcohols (*20*–*22*). In our efforts to develop alternative methods for the asymmetric synthesis of chiral amines, we recently achieved the enantioselective C–H iodination of triflyl-protected benzylamines by desymmetrization (*11*). This ligand-controlled reaction has recently been modified to achieve an atropselective C–H iodination through kinetic resolution in promising selectivity ($s \leq 27$) (*23*). To access a wide range of chiral α-branched benzylamines that do not contain two identical aryl groups, we embarked on the development of a kinetic resolution process through an enantioselective C–H iodination of arylalkylamines. Practically, this type of process would not only lead to the resolution of racemic amines but also concomitantly introduce a new functional handle for the further elaboration of the product. Conceptually, the chiral recognition required in kinetic resolution is fundamentally different from that in the desymmetrization process. The catalyst must preferentially recognize one of the enantiomeric substrates in kinetic resolution rather than one of the prochiral groups within the same substrate as in desymmetrization. We were inspired in this context by the landmark success in kinetic resolution of Jacobsen's cobalt-salen–catalyzed epoxide opening process (*24*). The Pd(II)-catalyzed asymmetric oxidation of racemic alcohols (*25*, *26*) has also been demonstrated. However, kinetic

The Scripps Research Institute, 10550 North Torrey Pines Road, La Jolla, CA 92037, USA.
*Corresponding author. E-mail: yu200@scripps.edu

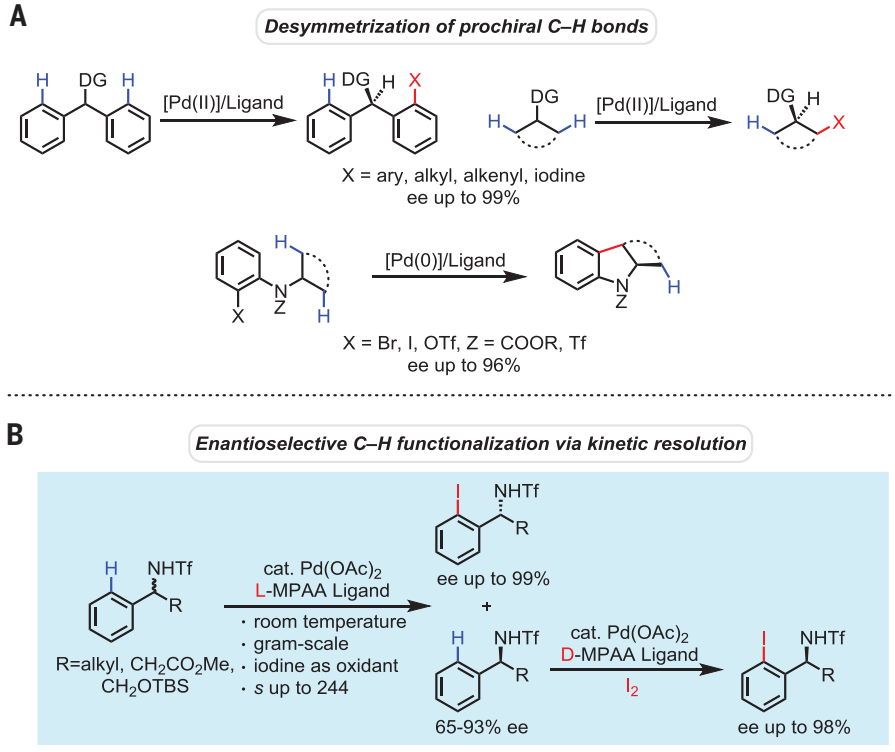


**Fig. 1. Enantioselective C–H activation reactions.** (**A**) Desymmetrization of prochiral C–H bonds. (**B**) Enantioselective C–H activation through kinetic resolution.

**Table 1. Enantioselective C–H iodination of benzylamines.**

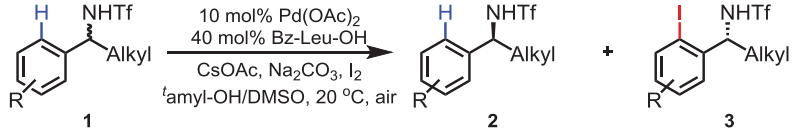


| entry | 1 | Ar | Alkyl | time (h) | conv.* (yield, %)† | ee(%)‡ 2 | ee(%)‡ 3 | s§ |
|---|---|---|---|---|---|---|---|---|
| 1‖ | **1a** | 2-Me-Ph | Me | 24 | 51 (48) | 93 | 91 | 73.6 |
| 2 | **1b** | 2-Me-Ph | Et | 24 | 50 (49) | 91 | 91 | 67.3 |
| 3 | **1c** | 2-Me-Ph | $^{n}$Bu | 48 | 47 (45) | 77 | 87 | 32.9 |
| 4 | **1d** | 2-Me-Ph | $^{i}$Bu | 48 | 51 (49) | 83 | 81 | 25.0 |
| 5 | **1e** | 2-Me-Ph | Bn | 48 | 47 (44) | 67 | 75 | 13.8 |
| 6 | **1f** | 2-Me-Ph | cyclopropyl | 24 | 42 (42) | 70 | 95 | 83.5 |
| 7 | **1g** | 2-OMe-Ph | Me | 24 | 49 (46) | 93 | 97 | 240 |
| 8 | **1h** | 2-F-Ph | Me | 24 | 48 (47) | 89 | 96 | 148 |
| 9 | **1i** | 2-Me,4-Cl-Ph | Me | 24 | 51 (49) | 97 | 93 | 113 |
| 10 | **1j** | 3-Me-Ph | Me | 24 | 45¶ (42, mono:di=3:1) | 78 | 92# | 99.5 |
| 11 | **1k** | 4-Me-Ph | Me | 48 | 45 (35) | 78 | 95 | 91.7 |
| 12 | **1l** | 2-naphthyl | Me | 48 | 41 (37) | 67 | 95 | 76.0 |
| 13** | **1m** | Ph | $^{n}$Bu | 48 | 42¶ (40, mono:di=1:1.4) | 70 | 87# (99††) | 124 |
| 14 | **1n** | Ph | $^{i}$Pr | 48 | 33 (30) | 45 | 90 | 34.5 |

*Calculated conversion, c = $ee_2$ / ($ee_2$ + $ee_3$). †Isolated yield of the iodinated product. ‡Determined by chiral HPLC analysis. §Selectivity(*s*) = (rate of fast-reacting enantiomer) / (rate of slow-reacting enantiomer). ‖Reaction also proceeds with 2 mol% $Pd(OAc)_2$ (see Table S1 in supplementary materials for details). ¶Determined by crude $^{1}$H-NMR. #ee for the mono product. **3 equiv. $I_2$ was added after 24 h. ††ee for the di product.

Downloaded from http://science.sciencemag.org/ on March 13, 2018

resolution via a Pd-catalyzed C–H activation reaction involving chiral C($sp^3$) centers remains to be established.

Here, we report the discovery of a highly efficient kinetic resolution of chiral amines by Pd-catalyzed C–H iodination with selectivities reaching up to 244 (Fig. 1B). In addition to simple arylalkylamines, a wide range of β-amino acids and β-amino alcohols are compatible with this reaction. The use of ambient temperature provides a major operational advantage over nonenzymatic acylative kinetic resolution reactions, which often require low temperature conditions. We further demonstrate that the remaining starting material can subsequently be iodinated using a chiral ligand with opposite configuration to give ortho-iodinated amines in high ees, thus rendering this method capable of converting both enantiomers of the racemic amines into ortho-iodinated chiral benzylamines. The newly introduced ortho-iodides are a useful functional handle, allowing conversion of the products into a broad range of chiral amines.

Our experimental design was based on a previous finding that a mono-protected amino acid ligand (MPAA) can effectively control the stereochemistry in Pd-catalyzed asymmetric insertion into prochiral C–H bonds on different carbon centers, leading to desymmetrization (*10*). This led us to hypothesize that the chiral catalyst assembled from the amino acid ligand and Pd(II) species could preferentially recognize one enantiomer of a racemic substrate during the C–H activation step. If successful, a wide range of C–H activation reactions could potentially be developed into practical tools for asymmetric catalysis through kinetic resolution. Due to its compatibility with low reaction temperatures, we selected our recently developed C–H iodination as a model reaction to investigate the feasibility of achieving kinetic resolution of α-branched benzylamines at room temperature. Thus, 1-(*o*-tolyl) ethylamine, protected by a triflyl group (**1a**), was subjected to our iodination conditions in the presence of various mono-protected amino acid ligands (see table S1). We found that using benzoyl-protected L-2-aminopentanoic acid (norvaline) as the chiral ligand, Pd(II)-catalyzed iodination of **1a** proceeded with promising selectivity (table S1, entry 1, $s$ = 17.6). A minor increase in steric hindrance on the side chain when leucine was used improved the selectivity to 50 (table S1, entries 2 and 3). However, further tuning the steric bulkiness of the side chain only afforded lower selectivity (table S1, entries 4 to 6). Extensive efforts to improve the selectivity by using a substituted *N*-benzoyl protecting group were unsuccessful (table S1, entries 7 to 12). We also found that acetyl, trifluoroacetyl, and Boc protecting groups were inferior to benzoyl-type protecting groups (table S1, entries 13 to 15). We further found that an increase in the reaction concentration improved the selectivity to 62.0 (table S1, entry 16). Finally, an optimum selectivity of 78.8 was obtained by running the reaction in a 5:2.2 ratio of $^t$amyl alcohol and dimethyl sulfoxide (table S1, entry 17). In this case, both the iodinated product and the recovered starting material were obtained with high enantioselectivity (92% ee) at 50% conversion. The reaction also proceeded with 2 mole percent Pd catalyst to reach a selectivity of 51.2, albeit at longer reaction times (table S1, entry 17). Reducing the ratio of ligand/Pd from 4:1 to 2:1 in the iodination of **1a** resulted in a significant drop of selectivity ($s$ = 33), which can be attributed to competitive binding of the substrate versus ligands (table S1, entry 18).

To examine whether this method could be applied to prepare a broad range of chiral ortho-iodinated benzylamines, we subjected amines **1b** to **1l** to the optimized conditions (Table 1). Iodination of benzylamines **1a** to **1c** gave good to excellent selectivity, whereas the bulkier α-isobutyl and benzyl groups in **1d** and **1e** led to decreases in the selectivity factor to 25.0 and 13.8, respectively (Table 1, entries 1 to 5). Iodination of benzylamine **1f** containing a cyclopropyl group proceeded with an excellent selectivity factor (entry 6, $s$ = 83.5). Arenes containing ortho-methoxy and fluoro groups were also iodinated with outstanding selectivity (entries 7 and 8, $s$ = 148 and 240, respectively). The presence of a para-chloro group on the aryl fragment in **1i** was well tolerated (entry 9, $s$ = 113). Meta- and para-methyl substituted arenes **1j** and **1k** were more suitable substrates than the ortho-methylarene **1a** affording excellent selectivity (entries 10 and 11, $s$ = 99.5 and 91.7, respectively). Iodination of **1l** containing 2-naphthyl group also proceeded with synthetically useful selectivity (entry 12, $s$ = 76). In general, the iodinated products were obtained with high levels of enantioselectivity (91 to 97% ee), with the exception of entries 3 to 5. To investigate whether the decrease of enantioselectivity with these substrates containing bulkier α-alkyls (entries 3 to 5) was a general phenomenon, we subjected **1m** containing α-butyl to the standard iodination conditions. The reaction proceeded with high selectivity (entry 13, $s$ = 124), thus suggesting that the observed adverse effect of the bulky α-alkyl group was partially due to the ortho-methyl groups in substrates **1a** to **1e**. However, the presence of an even bulkier α-*i*-propyl in substrate **1n** also reduced the selectivity to 34.5 (entry 14). Replacing the α-*i*-propyl with α-*t*-butyl resulted in a loss of reactivity under current conditions.

**Table 2. Enantioselective C–H iodination of β-amino acids and amino alcohols.**

**A**

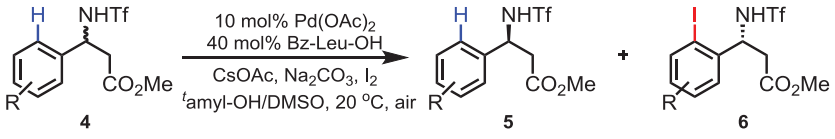


| entry | 4 | Ar | time (h) | conv.* (yield, %)† | ee(%)‡ 5 | ee(%)‡ 6 | s§ |
|---|---|---|---|---|---|---|---|
| 1 | **4a** | Ph | 48 | 47‖ (44, mono:di=2:1) | 85 | 96¶ | 128 |
| 2 | **4b** | 2-Me-Ph | 24 | 49 (49) | 93 | 96 | 168 |
| 3 | **4c** | 3-Me-Ph | 48 | 50 (44) | 93 | 94 | 112 |
| 4 | **4d** | 4-OMe-Ph | 48 | 46‖ (43, mono:di=3:1) | 82 | 98¶ | 134 |
| 5# | **4e** | 4-F-Ph | 48 | 48 (41) | 90 | 98 | 244 |
| 6# | **4f** | 4-Cl-Ph | 48 | 49 (40) | 92 | 97 | 152 |
| 7# | **4g** | 4-$CF_3$-Ph | 48 | 40 (38) | 65 | 99 | 155 |

*Calculated conversion, c = $ee_5$ / ($ee_5$ + $ee_6$). †Isolated yield of the iodinated product. ‡Determined by chiral HPLC analysis. §Selectivity($s$) = (rate of fast-reacting enantiomer) / (rate of slow-reacting enantiomer). ‖Determined by crude $^1$H-NMR. ¶ee for the mono product. #3 equiv. $I_2$ was added after 24 h.

**B**

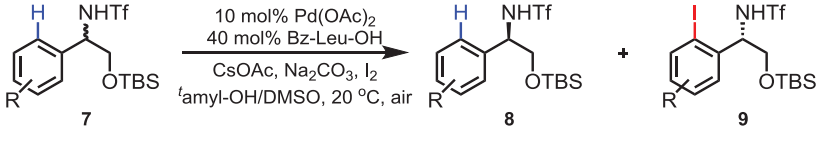


| entry | 7 | Ar | time (h) | conv. (yield, %) | ee(%) 8 | ee(%) 9 | s |
|---|---|---|---|---|---|---|---|
| 1 | **7a** | Ph | 48 | 43* (40, mono:di=1:1) | 71 | 87† (99‡) | 88.0 |
| 2 | **7b** | 2-Me-Ph | 48 | 50 (49) | 91 | 92 | 77.2 |
| 3 | **7c** | 2-F-Ph | 48 | 41 (41) | 68 | 99 | 188 |
| 4 | **7d** | 2-naphthyl | 48 | 43 (40) | 72 | 96 | 112 |

*Determined by crude $^1$H-NMR. †ee for the mono product. ‡ee for the di product.

Downloaded from http://science.sciencemag.org/ on March 13, 2018

We next investigated whether our enantioselective iodination could be applied to the production of iodinated chiral β-amino acids (Table 2A). In spite of a number of highly creative asymmetric methods for making enantioenriched β-amino acids (*27*), resolution is still frequently used in practice because of the ease of preparing racemic β-amino acids by the Rodionov reaction. The development of highly efficient catalysts to resolve racemic β-amino acids continues to attract considerable attention (*28*–*30*). Using our methodology, β-phenyl-β-amino acid **4a** was iodinated under the standard conditions to give **6a** with excellent selectivity (*s* = 128). Substrates containing electron-donating groups at the ortho, meta and para positions of the β-phenyl groups were all iodinated with high selectivity factors ranging from 112 to 168 (Table 2A, entries 2 to 4). Electron-withdrawing groups on the β-phenyl rings were also compatible with this transformation affording selectivity factors as high as 244 (entries 5 to 7). In all cases, the iodinated amino acid derivatives were obtained with high levels of enantioselectivity (94 to 99% ee).

We were pleased to find that this enantioselective C–H activation method was also suitable for preparing ortho-iodinated chiral β-amino alcohols (Table 2B). 2-Phenyl amino alcohol **7a** was iodinated with a practically useful selectivity (*s* = 88). The ortho-methyl group in **7b** led to a slight decrease in the selectivity factor (*s* = 77.2), whereas 2-(ortho-fluoro)-phenyl and 2-naphthyl-amino alcohols were iodinated with excellent selectivity (*s* = 188 and 112, respectively).

To further demonstrate the versatility of this kinetic resolution process, we developed a protocol to convert both enantiomers of the racemic amine substrates to the chiral-iodinated amines in high enantiomeric purity. Thus, 1.0 g of **1l** was subjected to the standard reaction conditions using the L-amino acid ligand to give 37% iodinated product **3l** (maximum 50% yield) with 95% ee (Fig. 2A). The absolute configuration of **3l** determined by x-ray crystallography should also facilitate future establishment of a stereomodel for kinetic resolution by C–H activation. The recovered starting material **2l** with 69% ee was then iodinated using the D-amino acid ligand to give chiral amine **3l′** in 98% ee (Fig. 2A). The use of ligands possessing the opposite configuration to enantioselectively iodinate the enantiomerically enriched starting material could prove extremely useful when the selectivity factor is lower than 50 and the ee of the starting material is lower than 90%. To render this reaction synthetically useful, triflyl-protected amine **3l** was readily deprotected and converted to benzoyl-protected amine **10** under mild conditions without racemization (Fig. 2B). Finally, the chiral-iodinated amine **3l** was converted to a diverse range of amines, illustrating the broad utility of this method to access a diverse range of chiral amines (Fig. 2C).

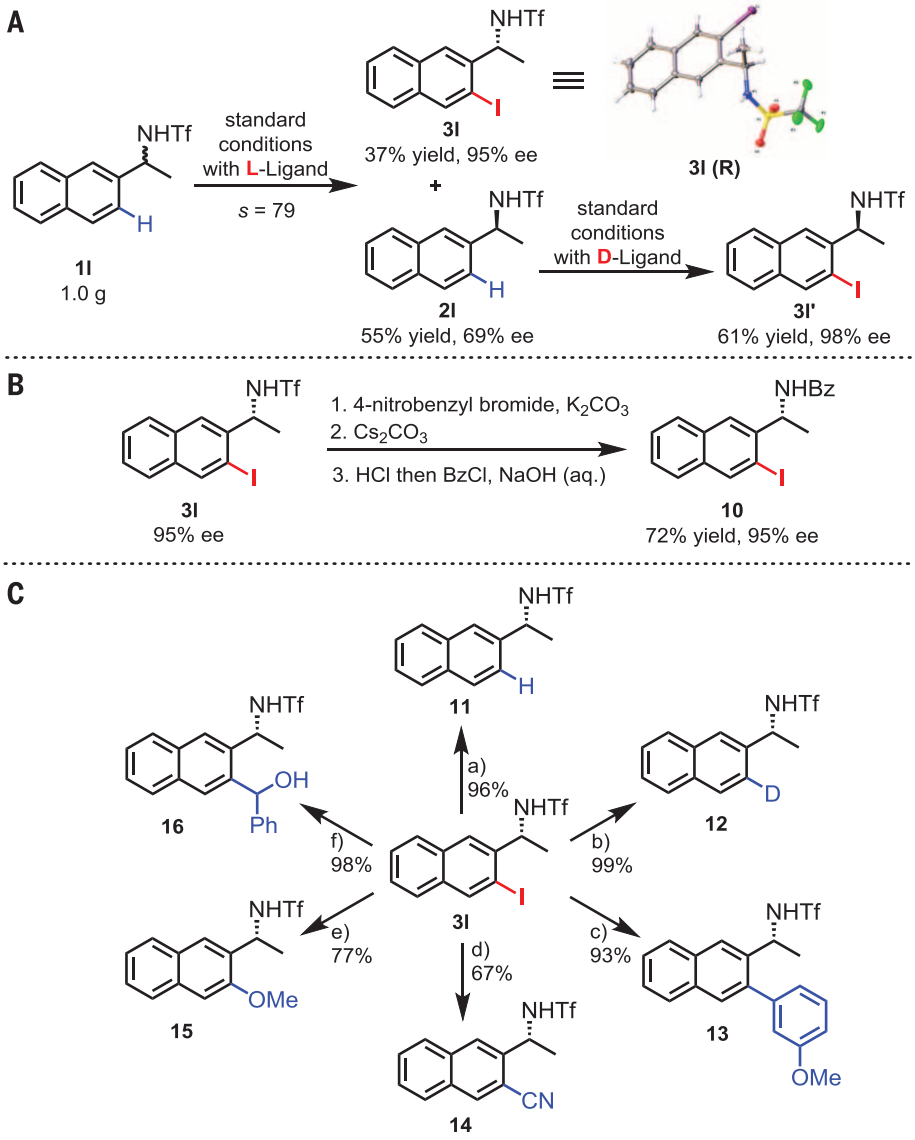


**Fig. 2. Enrichment and elaboration of products.** (**A**) Gram-scale synthesis, reaction with D-amino acid ligand and x-ray crystallography of **3l**. (**B**) Deprotection of the triflyl protecting group. (**C**) Functionalization of iodinated chiral amine **3l**. Reaction conditions: a) 5 mol% $Pd(PPh_3)_4$, $HCO_2Na$, dimethylformamide (DMF), 110°C; b) 1) $^i$PrMgCl-LiCl, tetrahedrofuran (THF), 0°C, 2) $D_2O$; c) 2.5 mol% $Pd(OAc)_2$, 5 mol% 2-dicyclohexylphosphino-2′,6′-dimethoxybiphenyl (S-Phos), 3-anisole-boronic-acid, $K_2CO_3$, acetonitrile/$H_2O$, 100°C; d) CuCN, L-proline, DMF, 120°C; e) 20 mol% CuI, 40 mol% 1,10-phenanthroline, $Cs_2CO_3$, MeOH, 110°C; f) 1) $^i$PrMgCl-LiCl, THF, 0°C, 2) PhCHO, 0°C to room temperature.

## REFERENCES AND NOTES


1. R. Giri, B.-F. Shi, K. M. Engle, N. Maugel, J.-Q. Yu, *Chem. Soc. Rev.* **38**, 3242–3272 (2009).
2. M. P. Doyle, R. Duffy, M. Ratnikov, L. Zhou, *Chem. Rev.* **110**, 704–724 (2010).
3. R. P. Reddy, H. M. L. Davies, *Org. Lett.* **8**, 5013–5016 (2006).
4. C. Liang *et al.*, *Angew. Chem. Int. Ed.* **45**, 4641–4644 (2006).
5. D. N. Zalatan, J. Du Bois, *J. Am. Chem. Soc.* **130**, 9220–9221 (2008).
6. E. Milczek, N. Boudet, S. Blakey, *Angew. Chem. Int. Ed.* **47**, 6825–6828 (2008).
7. T. K. Hyster, L. Knörr, T. R. Ward, T. Rovis, *Science* **338**, 500–503 (2012).
8. B. Ye, N. Cramer, *Science* **338**, 504–506 (2012).
9. F. Kakiuchi, P. L. Gendre, A. Yamada, H. Ohtaki, S. Murai, *Tetrahedron Asymmetry* **11**, 2647–2651 (2000).
10. B.-F. Shi, N. Maugel, Y.-H. Zhang, J.-Q. Yu, *Angew. Chem. Int. Ed.* **47**, 4882–4886 (2008).
11. L. Chu, X.-C. Wang, C. E. Moore, A. L. Rheingold, J.-Q. Yu, *J. Am. Chem. Soc.* **135**, 16344–16347 (2013).
12. M. Nakanishi, D. Katayev, C. Besnard, E. P. Kündig, *Angew. Chem. Int. Ed.* **50**, 7438–7441 (2011).
13. S. Anas, A. Cordi, H. B. Kagan, *Chem. Commun.* **47**, 11483–11485 (2011).
14. T. Saget, S. J. Lemouzy, N. Cramer, *Angew. Chem. Int. Ed.* **51**, 2238–2242 (2012).
15. D. Katayev, M. Nakanishi, T. Bürgi, E. P. Kündig, *Chem. Sci.* **3**, 1422–1425 (2012).
16. F. Schmidt, R. T. Stemmler, J. Rudolph, C. Bolm, *Chem. Soc. Rev.* **35**, 454–470 (2006).
17. M. T. Robak, M. A. Herbage, J. A. Ellman, *Chem. Rev.* **110**, 3600–3740 (2010).
18. J. Paetzold, J. E. Bäckvall, *J. Am. Chem. Soc.* **127**, 17620–17621 (2005).
19. M. Breuer *et al.*, *Angew. Chem. Int. Ed.* **43**, 788–824 (2004).
20. S. Arai, S. Bellemin-Laponnaz, G. C. Fu, *Angew. Chem. Int. Ed.* **40**, 234–236 (2001).
21. C. K. De, E. G. Klauber, D. Seidel, *J. Am. Chem. Soc.* **131**, 17060–17061 (2009).


Downloaded from http://science.sciencemag.org/ on March 13, 2018

22. B. S. Fowler, P. J. Mikochik, S. J. Miller, *J. Am. Chem. Soc.* **132**, 2870–2871 (2010).
23. D.-W. Gao, Q. Gu, S.-L. You, *ACS Catal.* **4**, 2741–2745 (2014).
24. M. Tokunaga, J. F. Larrow, F. Kakiuchi, E. N. Jacobsen, *Science* **277**, 936–938 (1997).
25. D. R. Jensen, J. S. Pugsley, M. S. Sigman, *J. Am. Chem. Soc.* **123**, 7475–7476 (2001).
26. E. M. Ferreira, B. M. Stoltz, *J. Am. Chem. Soc.* **123**, 7725–7726 (2001).
27. J. Song, Y. Wang, L. Deng, *J. Am. Chem. Soc.* **128**, 6048–6049 (2006).
28. A. Berkessel, F. Cleemann, S. Mukherjee, *Angew. Chem. Int. Ed.* **44**, 7466–7469 (2005).
29. V. D. Bumbu, V. B. Birman, *J. Am. Chem. Soc.* **133**, 13902–13905 (2011).
30. S. Zhou *et al.*, *Angew. Chem. Int. Ed.* **53**, 7883–7886 (2014).

**ACKNOWLEDGMENTS**

We gratefully acknowledge The Scripps Research Institute and NIH (National Institute of General Medical Sciences, 2R01GM084019) for financial support. J.-Q. Y. and L.C. conceived the concept. L.C. developed the enantioselective C–H iodination. L.C. and K.-J.X. synthesized the amine substrates. J.-Q.Y. directed the project. We thank J. Spangler for constructive suggestions. Metrical parameters for the structures of **3l** are available free of charge from the Cambridge Crystallographic Data Centre under reference number CCDC-1021096.

**SUPPLEMENTARY MATERIALS**

www.sciencemag.org/content/346/6208/451/suppl/DC1
Materials and Methods
Supplementary Text
Tables S1 and S2
References (*31*–*35*)

9 July 2014; accepted 5 September 2014
10.1126/science.1258538

METALLOPROTEINS

# Structural basis for organohalide respiration

**Martin Bommer,[1]* Cindy Kunze,[2]* Jochen Fesseler,[1] Torsten Schubert,[2] Gabriele Diekert,[2]† Holger Dobbek[1]†**

**Organohalide-respiring microorganisms can use a variety of persistent pollutants, including trichloroethene (TCE), as terminal electron acceptors. The final two-electron transfer step in organohalide respiration is catalyzed by reductive dehalogenases. Here we report the x-ray crystal structure of PceA, an archetypal dehalogenase from *Sulfurospirillum multivorans*, as well as structures of PceA in complex with TCE and product analogs. The active site harbors a deeply buried norpseudo-$B_{12}$ cofactor within a nitroreductase fold, also found in a mammalian $B_{12}$ chaperone. The structures of PceA reveal how a cobalamin supports a reductive haloelimination exploiting a conserved $B_{12}$-binding scaffold capped by a highly variable substrate-capturing region.**

Anaerobic microorganisms use alternative terminal electron acceptors during respiration, such as nitrate, sulfate, iron(III), or even organohalides. The accumulation of polluting organohalides such as perchloroethylene (PCE, also tetrachloroethene) and trichloroethene (TCE) in the environment, which have been heavily used for dry cleaning and degreasing, is problematic because of their toxicity; however, microbial organohalide respiration can transform these compounds into less toxic forms. Organohalide respiration requires reductive dehalogenases (RDases) for the central reduction step (*1*). In contrast to terminal reductases that contain prosthetic heme groups, molybdopterin, or flavins as cofactors, RDases harbor a corrinoid cofactor and two Fe/S clusters (*2*). RDases are able to convert some of the most noxious environmental pollutants, including halogenated phenols, dioxins, biphenyls, and aliphatic hydrocarbons. RDase genes were identified in distantly related bacterial genera belonging to the chloroflexi; firmicutes; gamma-, delta-, and epsilonproteobacteria; and even archaea (*3*).

[1]Institut für Biologie, Strukturbiologie/Biochemie, Humboldt-Universität zu Berlin, Unter den Linden 6, 10099 Berlin, Germany. [2]Institut für Mikrobiologie, Friedrich-Schiller-Universität Jena, Lehrstuhl für Angewandte und Ökologische Mikrobiologie, Philosophenweg 12, 07743 Jena, Germany.
*These authors contributed equally to this work. **†Corresponding author. E-mail: holger.dobbek@biologie.hu-berlin.de (H.D.); gabriele.diekert@uni-jena.de (G.D.)**

Several hundred RDase gene sequences deposited in databases await testing for functionality and determination of the substrate spectrum. Low growth yields and the oxygen sensitivity of the RDases have hindered large-scale purification and biochemical characterization of RDases (*1*). Genetic manipulation of the bacterial isolates has thus far been difficult, and only recently was functional heterologous production of RDases reported, but it remains challenging (*4*). Structural data will help to resolve how RDases evolved, function, and specifically select the many different substrates, some of which have been present in the biosphere for less than a century.

Here we report the crystal structure of a reductive dehalogenase, PceA (*5*), of the microaerophilic epsilonproteobacterium *Sulfurospirillum multivorans* (formerly *Dehalospirillum multivorans*) (*6*) (i) in an empty state; (ii) in the presence of TCE; (iii) in the presence of the *cis*-dichloroethene (*cis*-DCE) (product) analog *cis*-dibromoethene (*cis*-DBE); and (iv) in the presence of iodide, a substitute for the leaving chloride, at a maximum resolution of 1.6 Å (*7*). *S. multivorans* was isolated in the mid-1990s from activated sludge and possesses a flexible catabolism integrating numerous terminal reductases encoded in its genome (*8*). *S. multivorans* is able to couple the reductive dechlorination of PCE, TCE, or dibromoethene (DBE) to growth (*9*, *10*) through its prototypical RDase PceA.

The 464 amino acids of PceA are structured in a compact α/β fold domain (Fig. 1A). The structure can be divided into an N-terminal unit (residues 1 to 138), a norpseudo-$B_{12}$ binding core (residues 139 to 163 and 216 to 323), an insertion unit (residues 164 to 215), an iron-sulfur cluster binding unit (residues 324 to 394) and a C-terminal unit (residues 395 to 464) (fig. S1). Two protomers in the $P4_1$ asymmetric unit interact tightly to form a dimer with a twofold noncrystallographic symmetry. Two α helices of the norpseudo-$B_{12}$ binding core and one α helix of the N-terminal unit form a helical bundle with their symmetry mates. Along with extensive loop regions in the N- and C-terminal units, these bundles create the dimer interface. The interface covers 20% of the accessible surface area of the protomer, supporting a compact and stable dimeric arrangement. Using gel filtration, an apparent molecular mass of 89 kD (fig. S2) was determined for PceA purified from the membrane fraction, which agrees with a dimeric rather than a monomeric structure as reported previously for the soluble wild-type enzyme (*5*).

RDases lack obvious sequence similarities to other enzyme families, and the fold of PceA is unlike that of known corrinoid-dependent methyltransferases (*11*) or mutases (*12*). The most similar protein with clear homology found was methylmalonic aciduria *cblC* type with homocysteinuria (MMACHC) (*13*) (fig. S3). MMACHC is a $B_{12}$-trafficking chaperone essential for the formation of adenosyl- or methylcobalamin in humans by catalyzing the reductive removal of the upper axial ligands from cyanocobalamin and alkylcobalamins. Structural homology is limited to the $B_{12}$/norpseudo-$B_{12}$–binding core, which resembles the nitroreductase family fold (*14*) (fig. S3). Consequently, RDases and MMACHC most likely evolved from a common ancestral $B_{12}$-binding protein.

In addition to the norpseudo-$B_{12}$ cofactor, PceA also harbors two [4Fe-4S] clusters. Short distances between the two [4Fe-4S] clusters and the proximal [4Fe-4S] cluster and the Co bound to the corrin ring are expected to allow for a rapid electron transfer within a protein monomer (*15*) (Fig. 1B). The proximal [4Fe-4S] cluster is in van der Waals (vdW) contact distance to the C83 carboxamide side chain and C8 of the corrin ring [for atom numbering, see (*2*)], with the carboxamide N84 being in hydrogen bond distance to a μ3-sulfido ligand of the [4Fe-4S] cluster. The two active sites of the PceA dimer are at a Co-Co distance of 42 Å without cofactors between them, indicating two independent catalytic units per dimer (Fig. 1A).

Downloaded from http://science.sciencemag.org/ on March 13, 2018

Science

# Room-temperature enantioselective C–H iodination via kinetic resolution

Ling Chu, Kai-Jiong Xiao and Jin-Quan Yu

*Science* **346** (6208), 451-455.
DOI: 10.1126/science.1258538

**Ensuring handedness when breaking C-H bonds**

Many organic compounds are chiral: They manifest two distinct mirror-image variants, or enantiomers. Kinetic resolution can transform one enantiomer to a desired product while leaving its mirror image unmodified. Chu *et al.* applied this strategy to a reaction that replaces aryl carbon–hydrogen bonds with carbon-iodine bonds. They used a chiral palladium catalyst that reacts selectively with just one of two enantiomers of various benzylamine derivatives. In medicinal chemistry, such selective synthesis of individual enantiomers is essential for screening interactions with chiral biomolecules such as proteins.

*Science*, this issue p. 451

**ARTICLE TOOLS** http://science.sciencemag.org/content/346/6208/451

**SUPPLEMENTARY MATERIALS** http://science.sciencemag.org/content/suppl/2014/10/22/346.6208.451.DC1

**REFERENCES** This article cites 35 articles, 3 of which you can access for free
http://science.sciencemag.org/content/346/6208/451#BIBL

**PERMISSIONS** http://www.sciencemag.org/help/reprints-and-permissions

Use of this article is subject to the Terms of Service

*Science* (print ISSN 0036-8075; online ISSN 1095-9203) is published by the American Association for the Advancement of Science, 1200 New York Avenue NW, Washington, DC 20005. 2017 © The Authors, some rights reserved; exclusive licensee American Association for the Advancement of Science. No claim to original U.S. Government Works. The title *Science* is a registered trademark of AAAS.

Downloaded from http://science.sciencemag.org/ on March 13, 2018